Mapping Changes of Whole Brain Blood Flow in Rats with Myocardial Ischemia/Reperfusion Injury Assessed by Positron Emission Tomography*

Xu-chu PAN[1], Zhi-xiao LI[2], Duo-zhi WU[3], Shun-yuan LI[4], Hong-bing XIANG[2], Yong-tang SONG[1#]
[1]*Medical Association of Hubei Province, Wuhan 430071, China*
[2]*Department of Anesthesiology and Pain Medicine, Tongji Hospital, Tongji Medical College, Huazhong University of Science and Technology, Wuhan 430030, China*
[3]*Department of Anesthesiology, Hainan General Hospital, Haikou 570311, China*
[4]*Department of Anesthesiology, the First Affiliated Quanzhou Hospital of Fujian Medical University, Quanzhou 362000, China*

Summary: ^{18}F-labeled fluorodeoxyglucose positron emission tomography (^{18}F-FDG PET) is the most sensitive tool for studying brain metabolism *in vivo*. We investigated the image patterns of ^{18}F-FDG PET during reperfusion injury and correlated changes of whole brain blood flow utilizing a rat myocardial ischemia/reperfusion injury (MIRI) model. The results assessed by echocardiography indicated resultant cardiac dysfunction after ischemia-reperfusion in the rat heart. It was found that the average standardized uptake value ($SUV_{average}$) of the whole brain was significantly decreased in model rats, and the glucose uptake of different brain regions including accumbens core/shell (Acb), left caudate putamen (LCPu), hippocampus (HIP), left hypothalamus (LHYP), olfactory (OLF), superior colliculus (SC), right midbrain (RMID), ventral tegmental area (VTA), inferior colliculus (IC) and left thalamus whole (LTHA) was significantly decreased in MIRI rats whereas no significant difference was found in the $SUV_{average}$ of amygdala (AMY), right CPu, RHYP, right HYP, left MID, right THA, pons and medulla oblongata (MO). These ^{18}F-FDG PET data provide a reliable identification method for brain metabolic changes in rats with MIRI.
Key words: cardiac ischemia-reperfusion injury; brain metabolism; 18-fluorodeoxyglucose; positron emission tomography

The central nervous system is involved in the development and progression of myocardial ischemia-reperfusion injury (MIRI). Numerous researches have been performed to identify the changes of myocardial blood flow in coronary artery disease or cardiomyocyte damage by a positron emission tomography (PET) study[1–3], whereas reports about the changes of whole brain blood flow during cardiac ischemia are rare. A great need exists for improved brain-heart neural crosstalk[4–6], which is involved in an imbalance in metabolic supply and demand within the whole brain tissues, to offer potential information to further improve prognostic outcome of ischemic heart disease[7–10].

Xu-chu PAN, E-mail: panxuchu@sina.com
#Corresponding author, E-mail: yongtangsong@sina.com
*This project was supported by grants from National Natural Science Foundation of China (No. 81670240 and No. 81873467), National Natural Science Foundation of Hubei Province (No. 2016CFB625), Medical Innovation Project in Fujian Province (No. 2017-CX-48), and Key Research and Development Project of Hainan Province of China (No. ZDYF2018115).

Among all noninvasive imaging techniques, ^{18}F-labeled fluorodeoxyglucose (^{18}F-FDG) PET is a highly sensitive method for studying brain function *in vivo*[9, 11–14]. PET has revolutionized our understanding for the mechanism of ischemic heart disease[15–19], allowing the opportunity to investigate the metabolic mechanisms of brain-heart crosstalk by measuring the changes in regional cerebral blood flow or carbohydrate metabolism, and to prevent the myocardial tissues from reperfusion damage caused by myocardial ischemia. It is now widely recognized that ^{18}F-FDG reflects glucose flux and the applications of an ^{18}F-labeled perfusion agent have revealed details on the pathophysiology of brain diseases by measuring the regional cerebral metabolic rate of glucose[20–24]. For this purpose we mapped relative changes in regional cerebral blood flow (rCBF) induced by MIRI, using the technique of PET.

1 MATERIALS AND METHODS

1.1 Animals and Ethic Statement

Experimental protocols were approved by Local

Institutional Animal Care and Use Committee (IRBID: TJ-A20150804). Male adult SD rats (250–300 g) were purchased from the Experimental Animal Center of Tongji Medical College (China). Animals were fed and housed according to the guidelines of the National Institutes of Health Guide for the Care and Use of Laboratory Animals.

1.2 Experimental Design and Establishment of MIRI Model

Rats were divided into two groups: model group (n=10) and control group (n=10). To make MIRI rat model, we followed a previously reported procedure[25–29]. After rats were anesthetized, intubated, and ventilated with mixed air/oxygen, surgical thoracotomy was done. In model operations, the left anterior descending coronary artery (LAD) was ligated 2 mm below the left atrial appendage for 30 min and then reperfused for 2 h, whereas sutures were placed without LAD ligation in control operations. The core temperature was maintained throughout the protocol. Rats were monitored to confirm ischemic ST segment elevation during LAD occlusion by an electrocardiogram. Serum troponin cTnl of two groups was measured 2 h after reperfusion as an index of myocardial necrosis.

1.3 Echocardiography

Cardiac function was assessed after 30 min of LAD occlusion and 2 h of reperfusion using echocardiography. The rats were anesthetized with 1.5%–2.1% (v/v) isoflurane, operated and constant temperature was kept with heating blanket as described above[30, 31]. A transthoracic two-dimensional M-mode echocardiogram was used to measure the rat cardiac function in two groups. M-mode tracings were used to measure left ventricular end-systolic diameter (LVESD) and left ventricular end-diastolic diameter (LVEDD) according to the previously described data[32]. Left ventricular fractional shortening (LVFS) was calculated as follows: LVFS=(LVEDD–LVESD)/LVEDD×100%. The left ventricular ejection fraction (LVEF) was calculated from LV end-diastolic volume (LVEDV) and end-systolic volume (LVESD) using the equation of (LVEDV–LVESV)/LVEDV×100%.

1.4 Small-animal PET Imaging *In Vivo*

Before PET imaging, all rats were fasted overnight. Then the rats underwent surgical operation. At 90 min of reperfusion, approximately 500±50 μCi ^{18}F-FDG was injected via the tail vein. After 60 min of ^{18}F-FDG uptake, rats were anesthetized with 2% isoflurane. Images were obtained with the whole body scanning pattern (5 min per scanning bed) by the Trans-PET BioCaliburn 700 system (Raycan Technology Co., China). After imaging, animals were placed in an electric blanket until awake, then placed in an isolation room for 24 h to eliminate radiation hazards.

The PET images were reconstructed using the three-dimensional (3D) OSEM method with a voxel size of 0.5 mm×0.5 mm×0.5 mm, and were displayed in three planes: transverse, coronal, and sagittal planes. A volume-of-interest (VOI) analysis was conducted using the AMIDE software package (The Free Software Foundation Inc., USA). The maximum standardized uptake value (SUV_{max}) and average standardized uptake value ($SUV_{average}$) were calculated using the following formula: maximum pixel value with the decay-corrected region-of-interest activity (μCi/kg)/(injected dose[μCi]/weight[kg]).

1.5 Statistical analyses

All values were expressed as mean±SEM. GraphPad Prism software (GraphPad Software, Inc., USA) was used for statistical analysis. ANOVA test was used for comparison of 2 groups. A P value less than 0.05 was considered statistically significant.

2 RESULTS

2.1 Evaluation of MIRI Rat Models

We used the ECG to confirm the different stages of MIRI. In addition, serum cardiac troponin cTnl in model group was increased significantly as compared with that in control group. These results verified the successful establishment of MIRI model in the rats in this study.

2.2 Cardiac Function Assessed by Echocardiography

Regional left ventricular contractile function/LVFS *in vivo* after 30 min of LAD ligation and 2 h of reperfusion was assessed by echocardiography. Representative M-mode echocardiograms and corresponding values for LVEF are shown in fig. 1A (control group) and fig. 1B (model group). In model group, LVEF was significantly lower after ischemia-reperfusion than baseline (P<0.01), and LVFS was significantly lower after ischemia-reperfusion than baseline (P<0.001) (fig. 1C). Taken together, these results indicate that there is resultant cardiac dysfunction after ischemia-reperfusion in the rat heart.

2.3 PET for Whole Brain Blood Flow after MIRI

To assess whole brain blood flow, ^{18}F-FDG was used. Despite the uniform handling of the animals, there was high variability in uptake of ^{18}F-FDG from one mouse to the next. Correlation analysis indicated that the $SUV_{average}$ of the whole brain was significantly decreased in model rats, and the glucose uptake of different brain regions including accumbens (Acb), left caudate putamen (LCPu), hippocampus (HIP), left hypothalamus (LHYP), olfactory (OLF), superior colliculus (SC), right midbrain (RMID), ventral tegmental area (VTA), inferior colliculus (IC) and left thalamus vhole (LTHA) was significantly decreased in MIRI rats whereas no significant difference was found in the $SUV_{average}$ of amygdala (AMY), right CPu, right HYP, left MID, right THA, pons and medulla oblongata (MO) (fig. 2).

3 DISCUSSION

In the current study, a cardiac ischemia and reperfusion animal model was successfully verified, which was consistent with previous reports[28, 29, 33–35], and the efficiency of this method was also assessed by echocardiography. PET showed that FDG uptake in the whole brain in living rats exhibited a significant change 2.5 h after myocardial ischemia-reperfusion, suggesting that the redistribution of brain blood flow has important implications for the development of cardiac ischemia/reperfusion injury.

As the sensory stimulus is related to angina pectoris attack, cardiac ischemia may be assumed to reflect the circuitry involved in cardiovascular control[2, 36, 37]. We found that the glucose uptake of thalamus was

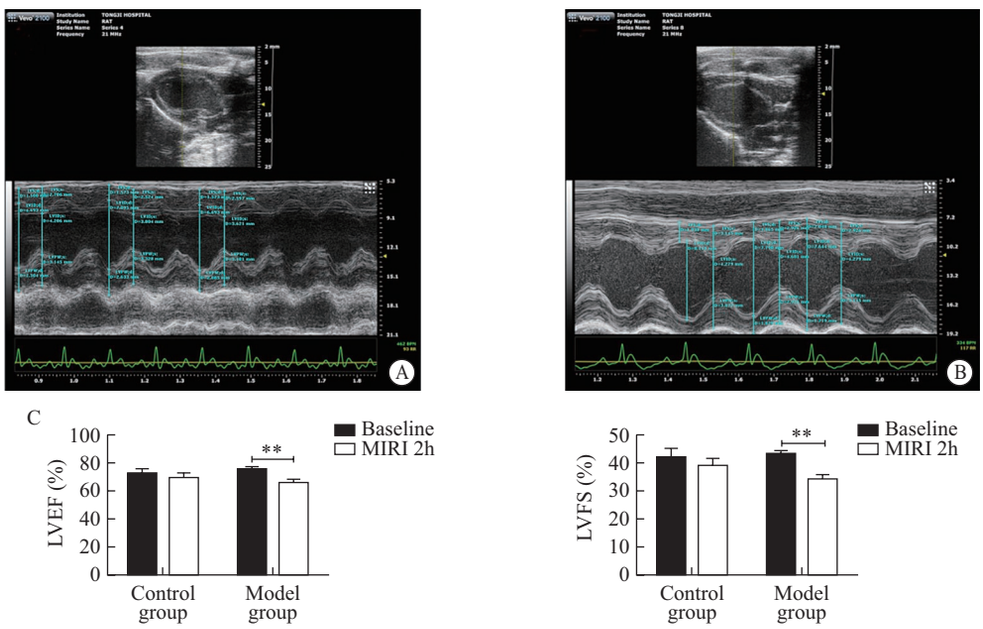

Fig. 1 Cardiac function assessed by echocardiography

A: representative M-mode echocardiograms in control group; B: representative M-mode echocardiograms in model group; C: LVEF(%) (left) and LVFS(%) (right) in control and model groups. Average data of LVEF and LVFS were assessed by echocardiography in male SD rats. n=4 rats per group. Results were expressed as mean±SEM. $^{**}P$<0.01. Student's t-test

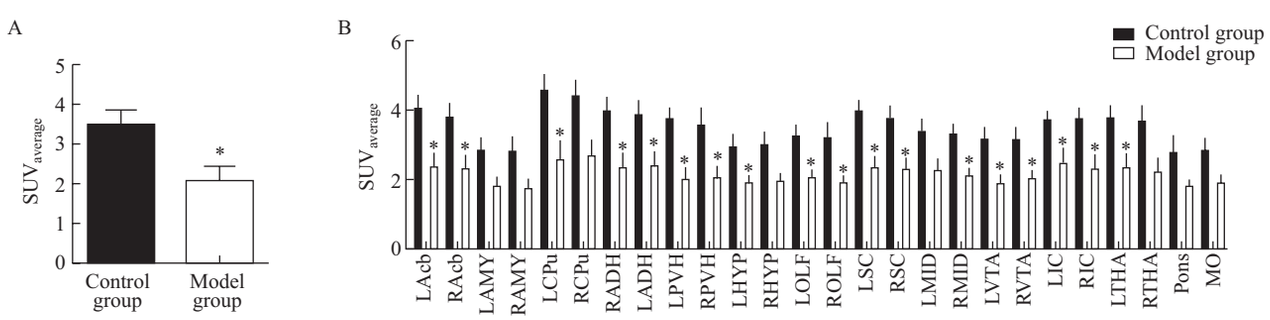

Fig. 2 The changes of glucose uptake in brain regions of myocardial ischemia reperfusion injury (MIRI) rats by small-animal PET scanning

A: The average glucose uptake of the whole brain is significantly decreased in model rats; B: The glucose uptake of different brain regions (Acb, LCPu, HIP, LHYP, OLF, SC, RMID, VTA , IC and LTHA) is significantly decreased in MIRI rats, whereas no significant difference was found in AMY, RCPu, RHYP, LMID, RTHA, pons and MO. Values are expressed as means±SEM, n=6 rats per group. $^{*}P$<0.05 *vs.* control group. LAcb: left accumbens core/shell; RAcb: right accumbens core/shell; LAMY: left amygdala; RAMY: right amygdala; LCPu: left caudate putamen; RCPu, right caudate putamen; LADH: left anterodorsal hippocampus; RADH: right anterodorsal hippocampus; LPVH: left posteroventral hippocampus; RPVH: right posteroventral hippocampus; LHYP: left hypothalamus; RHYP: right hypothalamus; LOLF: left olfactory; ROLF: right olfactory; LSC: left superior colliculus; RSC: right superior colliculus; LMID: left midbrain; RMID: right midbrain; LVTA: left ventral tegmental area; RVTA: right ventral tegmental area; LIC: left inferior colliculus; RIC: right inferior colliculus; LTHA: left thalamus whole; RTHA: right thalamus whole; MO: medulla oblongata

significantly decreased after MIRI, which was in line with a previous study showing that spinal cord stimulation applied at T1 thoracic segment resulted in the increased rCBF of the bilateral dorsomedial thalamus for acting a neurally mediated anti-anginal effect[36]. Guo *et al* investigated the potential existence of the response of neurons in the parafascicular nucleus of the thalamus to acute myocardial ischaemia induced by selective coronary artery occlusion, and observed that the discharge rate of these neurons was markedly increased following coronary artery occlusion, suggesting that the parafascicular nucleus of the thalamus may be involved in the modulation of cardiac nociception[6, 38]. Previous studies demonstrated that thalamic nucleus had an important "gate" function in the mediation of pain including cardiac ischemic pain[39–43], therefore, so changes in thalamic rCBF resulting from LAD ligation in our rat group may indicate the opening of this gate during myocardial ischemia.

The midbrain is another cerebral structure related to cardiovascular regulation. We found that the glucose uptake of midbrain was significantly decreased after MIRI, which was in agreement with a previous report in which T1 spinal cord stimulation induced the increased rCBF of the ventrolateral part of the periaqueductal grey[36], suggesting that there may exist the direct neuronal circuit from the periaqueductal grey to the heart. Our previous study reported that injection of pseudorabies virus (PRV) into the left ventricular wall resulted in the retrograde infection of neurons in the intermediolateral column of the spinal cord (IML), rostral ventrolateral reticular nucleus (RVLM), and the midbrain periaqueductal graymatter (PAG) through the sympathetic pathway[44], suggesting that the PAG-RVLM-IML pathway of synaptically connected neurons extends to the heart through sympathetic signaling. Lindberg *et al* confirmed previously described projection patterns of the PAG-RVLM axis and reported that the sympathetic efferent traveled caudally through the PAG and eventually reached the caudal autonomic centers including the C1 catecholamine cell group of the RVLM, indicating the existence of a formerly sympathetic projection pathway to a number of autonomic centers in the PAG[45]. These data suggested that the PAG rCBF resulting from LAD ligation in our rat group may be involved in the regulation of the cardiac sympathetic afferent reflex.

In conclusion, these ^{18}F-FDG PET data provide a reliable identification method for brain metabolic changes in rats with MIRI, and also offer a better understanding of the whole brain neural circuits innervating heart tissues, clearly demonstrating the rodent thalamus and midbrain regions involving in the control of the heart. Altogether, these data may help provide further rationale for the potential target related to brain metabolic changes for the treatment of some heart diseases.

Conflict of Interest Statement

The authors have no conflicts of interest related to this paper.

REFERENCES

1 Wang Q, He ZG, Li SY, *et al*. Application of animal and human PET in cardiac research. Am J Cardiovasc Dis, 2018,8(3):24-30

2 Hautvast RW, Blanksma PK, DeJongste MJ, *et al*. Effect of spinal cord stimulation on myocardial blood flow assessed by positron emission tomography in patients with refractory angina pectoris. Am J Cardiol, 1996,77(7):462-467

3 Blanksma PK, Pruim J. Positron emission tomography: measurement of myocardial perfusion using (13) N-labeled ammonia and (15)O-labeled water. Methods, 2002,27(3):226-227

4 Mazzeo AT, Micalizzi A, Mascia L, *et al*. Brain-heart crosstalk: the many faces of stress-related cardiomyopathy syndromes in anaesthesia and intensive care. Br J Anaesth, 2014,112(5):803-815

5 Ai J, Epstein PN, Gozal D, *et al*. Morphology and topography of nucleus ambiguus projections to cardiac ganglia in rats and mice. Neuroscience, 2007,149(4):845-860

6 Chen M, He ZG, Liu BW, *et al*. Parafascicular nucleus-heart neural crosstalk: Implications for seizure-induced myocardial stunning. Epilepsy Behav, 2016,63(1):135-137.

7 Schindler TH. Positron-emitting myocardial blood flow tracers and clinical potential. Prog Cardiovasc Dis, 2015,57(6):588-606

8 Bergstrom M, Awad R, Estrada S, *et al*. Autoradiography with positron emitting isotopes in positron emission tomography tracer discovery. Mol Imaging Biol, 2003,5(6):390-396

9 Hoff SJ, Stewart JR, Frist WH, *et al*. Noninvasive detection of heart transplant rejection with positron emission scintigraphy. Ann Thorac Surg, 1992,53(4):572-577

10 Srivatsava MK, Indirani M, Sathyamurthy I, *et al*. Role of PET-CT in the assessment of myocardial viability in patients with left ventricular dysfunction. Indian Heart J, 2016,68(5):693-699

11 Welch A, Mingarelli M, Riedel G, *et al*. Mapping changes in mouse brain metabolism with PET/CT. J Nucl Med, 2013,54(11):1946-1953

12 Daly KP, Dearling JL, Seto T, *et al*. Use of [18F] FDG Positron Emission Tomography to Monitor the Development of Cardiac Allograft Rejection. Transplantation, 2015,99(9):e132-139

13 van der Veen DR, Shao J, Chapman S, *et al*. A 24-hour temporal profile of in vivo brain and heart pet imaging reveals a nocturnal peak in brain 18F-fluorodeoxyglucose uptake. PLoS One, 2012,7(2):e31792

14 Kornblum HI, Araujo DM, Annala AJ, *et al*. In vivo imaging of neuronal activation and plasticity in the rat brain by high resolution positron emission tomography (microPET). Nat Biotechnol, 2000,18(6):655-660

15 Pirich C, Schwaiger M. The clinical role of positron emission tomography in management of the cardiac

patient. Rev Port Cardiol, 2000,19 Suppl 1:I89-100
16 Elsinga PH, Doze P, van Waarde A, *et al*. Imaging of beta-adrenoceptors in the human thorax using (S)-[(11) C]CGP12388 and positron emission tomography. Eur J Pharmacol, 2001,433(2-3):173-176
17 Meeder JG, Peels HO, Blanksma PK, *et al*. Comparison between positron emission tomography myocardial perfusion imaging and intracoronary Doppler flow velocity measurements at rest and during cold pressor testing in angiographically normal coronary arteries in patients with one-vessel coronary artery disease. Am J Cardiol, 1996,78(5):526-531
18 Meeder JG, Blanksma PK, van der Wall EE, *et al*. Coronary vasomotion in patients with syndrome X: evaluation with positron emission tomography and parametric myocardial perfusion imaging. Eur J Nucl Med, 1997,24(5):530-537
19 Meeder JG, Blanksma PK, van der Wall EE, *et al*. Long-term cigarette smoking is associated with increased myocardial perfusion heterogeneity assessed by positron emission tomography. Eur J Nucl Med, 1996,23(11):1442-1447
20 Tian XB, Li RC, Bu HL, *et al*. The mechanism of electroacupuncture for predicting the efficacy of deep brain stimulation in pharmacoresistant epilepsy may be involved in the melanocortinergic signal. Epilepsy Behav, 2013,29(3):594-596
21 Tian XB, Feng J, Bu HL, *et al*. The change in cerebral glucose metabolism generated by electroacupuncture may predict the outcome of stimulation of the anterior nucleus thalamus in refractory epilepsy. Epilepsy Behav, 2013,29(2): 427-429
22 Qiu Q, Li RC, Ding DF, *et al*. Possible mechanism of regulating glucose metabolism with subthalamic nucleus stimulation in Parkinson's disease: a virally mediated trans-synaptic tracing study in transgenic mice. Parkinsonism Relat Disord, 2014,20(4):468-470
23 Lee WW. Recent Advances in Nuclear Cardiology. Nucl Med Mol Imaging, 2016,50(3):196-206
24 Nagaoka T, Katayama Y, Kano T, *et al*. Changes in glucose metabolism in cerebral cortex and cerebellum correlate with tremor and rigidity control by subthalamic nucleus stimulation in Parkinson's disease: a positron emission tomography study. Neuromodulation, 2007,10(3):206-215
25 Qi D, Hu X, Wu X, *et al*. Cardiac macrophage migration inhibitory factor inhibits JNK pathway activation and injury during ischemia/reperfusion. J Clin Invest, 2009,119(12):3807-3816
26 Wang Q, Li ZX, Li YJ, *et al*. Identification of lncRNA and mRNA expression profiles in rat spinal cords at various time points following cardiac ischemia/reperfusion. Int J Mol Med, 2019,43(6):2361-2375
27 Wang Q, Li ZX, Li YJ, *et al*. Alterations in amino acid levels and metabolite ratio of spinal cord in rat with myocardial ischemia-reperfusion injury by proton magnetic resonance spectroscopy. Am J Transl Res, 2019,11(5):3101-3108
28 Wang Q, He ZG, Li ZX, *et al*. Bioinformatics analysis of gene expression profile data to screen key genes involved in cardiac ischemia-reperfusion injury. Int J Clin Exp Med, 2018,11(5):4955-4966
29 Xu AJ, Song ZP, Peng YW, *et al*. Change of mitochondrial function in the early stage after cardiac ischemia-reperfusion injury in mice. Int J Clin Exp Med, 2016,9(2):2549-2554
30 Hedhli N, Huang Q, Kalinowski A, *et al*. Endothelium-derived neuregulin protects the heart against ischemic injury. Circulation, 2011,123(20):2254-2262
31 Qi D, Atsina K, Qu L, *et al*. The vestigial enzyme D-dopachrome tautomerase protects the heart against ischemic injury. J Clin Invest, 2014,124(8):3540-3550
32 Li J, Qi D, Cheng H, *et al*. Urocortin 2 autocrine/paracrine and pharmacologic effects to activate AMP-activated protein kinase in the heart. Proc Natl Acad Sci USA, 2013,110(40):16 133-16 138
33 Huang CH, Lai CC, Yang AH, *et al*. Myocardial preconditioning reduces kidney injury and apoptosis induced by myocardial ischaemia and reperfusion. Eur J Cardio-thorac Surg, 2015,48(3):382-391
34 Borst O, Ochmann C, Schonberger T, *et al*. Methods employed for induction and analysis of experimental myocardial infarction in mice. Cell Physiol Biochem, 2011,28(1):1-12
35 Pisarenko OI, Shulzhenko VS, Studneva IM, *et al*. Signaling pathways of a structural analogue of apelin-12 involved in myocardial protection against ischemia/reperfusion injury. Peptides, 2015,73:67-76
36 Hautvast RW, Ter Horst GJ, DeJong BM, *et al*. Relative changes in regional cerebral blood flow during spinal cord stimulation in patients with refractory angina pectoris. Eur J Neurosci, 1997,9(6):1178-1183
37 Wang JP, Guo Z. Propofol suppresses activation of the nociception specific neuron in the parafascicular nucleus of the thalamus evoked by coronary artery occlusion in rats. Eur J Anaesthesiol, 2009,26(1):60-65
38 Guo Z, Yuan DJ. Midazolam inhibits cardiac nociception evoked by coronary artery occlusion in rats. Eur J Anaesthesiol, 2008,25(6):479-484
39 Zhu Q, Wu DC, Zhou XP, *et al*. Inhibitory effect of crotoxin on the pain-evoked discharge of neurons in thalamic parafascicular nucleus in rats. Toxicon, 2008,51(1):102-111
40 Cronin CC. Central nervous system pathways mediating angina pectoris. Lancet, 1994,344(8927):965
41 Channer KS. Central nervous system pathways mediating angina pectoris. Lancet, 1994,344(8927):964-965
42 Rosen SD, Paulesu E, Frith CD, *et al*. Central nervous pathways mediating angina pectoris. Lancet, 1994,344(8916):147-150
43 Cheng YF, Chang YT, Chen WH, *et al*. Cardioprotection induced in a mouse model of neuropathic pain via anterior nucleus of paraventricular thalamus. Nat Commun, 2017,8(1):826
44 Xu LJ, Liu TT, He ZG, *et al*. Hypothesis: CeM-RVLM circuits may be implicated in sudden unexpected death in epilepsy by melanocortinergic-sympathetic signaling. Epilepsy Behav, 2015,45:124-127
45 Lindberg D, Chen P, Li C. Conditional viral tracing reveals that steroidogenic factor 1-positive neurons of the dorsomedial subdivision of the ventromedial hypothalamus project to autonomic centers of the hypothalamus and hindbrain. J Comp Neurol, 2013,521(14):3167-3190

(Received Jan. 28, 2019; revised June 6, 2019)